C Journal of Carbon Research

MDPI

Article

Thermochemistry of the Smallest Hyperbolic Paraboloid Hydrocarbon: A High-Level Quantum Chemical Perspective

Amir Karton

School of Science and Technology, University of New England, Armidale, NSW 2351, Australia; amir.karton@une.edu.au

Abstract: [5.5.5.5]hexaene is a [12]annulene ring with a symmetrically bound carbon atom in its center. This is the smallest hydrocarbon with a hyperbolic paraboloid shape. [5.5.5.5]hexaene and related hydrocarbons are important building blocks in organic and materials chemistry. For example, penta-graphene—a puckered 2D allotrope of carbon—is comprised of similar repeating subunits. Here, we investigate the thermochemical and kinetic properties of [5.5.5.5]hexaene at the CCSD(T) level by means of the G4 thermochemical protocol. We find that this system is energetically stable relative to its isomeric forms. For example, isomers containing a phenyl ring with one or more acetylenic side chains are higher in energy by ΔH_{298} = 17.5–51.4 kJ mol^{-1}. [5.5.5.5]hexaene can undergo skeletal inversion via a completely planar transition structure; however, the activation energy for this process is $\Delta H^{\ddagger}_{298}$ = 249.2 kJ mol^{-1} at the G4 level. This demonstrates the high configurational stability of [5.5.5.5]hexaene towards skeletal inversion. [5.5.5.5]hexaene can also undergo a π-bond shift reaction which proceeds via a relatively low-lying transition structure with an activation energy of $\Delta H^{\ddagger}_{298}$ = 67.6 kJ mol^{-1}. Therefore, this process is expected to proceed rapidly at room temperature.

Keywords: penta-graphene; 2D Carbon allotrope; skeletal inversion; π-bond shift; CCSD(T); G4 theory

check for updates

Citation: Karton, A. Thermochemistry of the Smallest Hyperbolic Paraboloid Hydrocarbon: A High-Level Quantum Chemical Perspective. *C* **2023**, *9*, 41. https://doi.org/10.3390/c9020041

Academic Editor: Cédric Pardanaud

Received: 18 January 2023
Revised: 7 April 2023
Accepted: 10 April 2023
Published: 19 April 2023

Copyright: © 2023 by the author. Licensee MDPI, Basel, Switzerland. This article is an open access article distributed under the terms and conditions of the Creative Commons Attribution (CC BY) license (https://creativecommons.org/licenses/by/4.0/).

1. Introduction

Carbon atoms that are surrounded by an annulene ring have attracted considerable attention over the past 50 years [1–5]. A [12]annulene with a symmetrically bound carbon in its center is of particular importance since it adopts a hyperbolic paraboloidal shape due to a central sp^3 carbon surrounded by 12 sp^2 carbons. Scheme 1 illustrates the hyperbolic paraboloidal structure of the [12]annulene–[5.5.5.5]hexaene (**1**). In this structure, the central sp^3 carbon is located at the saddle point of the surface created by the four adjacent pentagons. It is well known that hyperbolic paraboloid surfaces of the equation $z = axy$ possess rigidity in the x and y directions [6,7]. Indeed, this may explain the high rigidity of penta-graphene—a two-dimensional allotrope of carbon. Penta-graphene, which consists of repeating hyperbolic paraboloid units, each comprising four pentagon rings sharing a vertex, has been suggested to be more rigid than graphene [8,9].

Computational quantum chemistry is a branch of chemistry that uses computational simulations to study the chemical properties of molecules and materials [10,11]. Computational quantum chemistry provides means for the rational design and development of new molecules and materials with tailored chemical properties. Due to significant advances in quantum theory and supercomputers, computational simulations are capable of unprecedented predictive accuracy. The present work focuses on the structural, thermodynamic, and kinetic properties of [5.5.5.5]hexaene. In particular, we use high-level composite ab initio methods [12,13] to show that [5.5.5.5]hexaene is (i) configurationally stable with respect to structural inversion, (ii) energetically stable relative to its isomeric forms, and (iii) has a relatively low lying π-bond shift transition state.

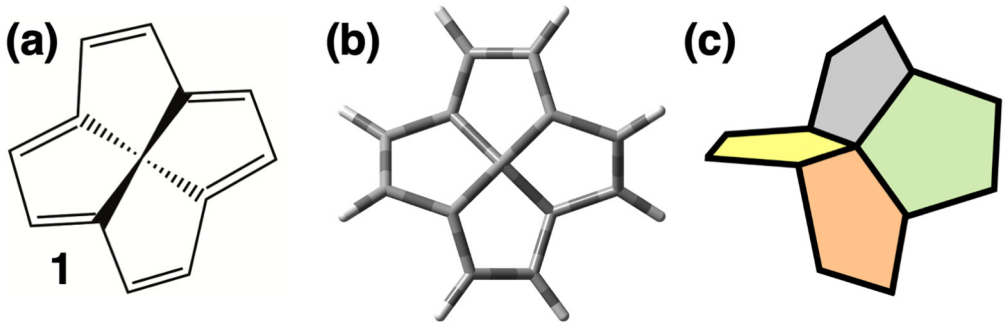

Scheme 1. (**a**) Skeletal structure of a hyperbolic paraboloidal shape created by four pentagon rings sharing a common vertex, (**b**) the optimized structure of [5.5.5.5] hexaene, and (**c**) a 3D representation of the hyperbolic paraboloidal structure.

2. Computational Details

In order to obtain accurate thermochemical and kinetic properties for the hydrocarbons considered in the present work, calculations have been carried out using the high-level, ab initio, G4 and G4(MP2) procedures [14–16]. These procedures combine coupled-cluster with single, double, and perturbative triple excitation (CCSD(T)) calculations as well as second- and fourth-order Møller–Plesset perturbation theories to approximate the CCSD(T) energy in conjunction with a triple-ζ-quality basis set (CCSD(T)/TZ). Both theories have been found to provide thermochemical and kinetic properties for hydrocarbons with chemical accuracy (arbitrarily defined as 1 kcal mol^{-1} = 4.2 kJ mol^{-1}) [14–27]. G4 theory is computationally more demanding and in most cases more accurate than G4(MP2) theory; therefore, the main text reports the G4 results whilst the G4(MP2) results are provided as Supporting Information. The geometries of all structures have been obtained at the B3LYP/6-31G(2df,p) level of theory [28–30] as prescribed in the G4 and G4(MP2) protocols. Harmonic vibrational frequencies have been calculated at the same level of theory to confirm that all stationary points are equilibrium structures (i.e., with all real frequencies) or transition structures (i.e., with one imaginary frequency). The connectivity of the transition structures were confirmed by performing intrinsic reaction coordinate calculations [31,32]. Zero-point vibrational energies and enthalpic temperature corrections have been obtained from the harmonic frequencies and scaled by appropriate scaling factors as recommended in G4 and G4(MP2) theories [15,16]. All DFT and ab initio calculations were performed using the Gaussian 09 program suite [33].

We have additionally assessed several DFT functionals for their ability to compute the isomerization energies of the highly unsaturated $C_{13}H_8$ isomers considered in the present work relative to the bottom-of-the-well G4 reference values. The considered DFT methods, ordered by their rung on Jacob's ladder [34], are the generalized gradient approximation (GGA) functionals BLYP [28,35], PBE [36], BPBE [35,36] and BP86 [35,37] the meta-GGA functionals TPSS [38] and MN15-L [39] the hybrid-GGAs B3LYP [28–30] B3PW91 [27,40], PBE0 [41] and the range-separated CAM-B3LYP [42] the hybrid-meta GGAs M05-2X [43], M06-2X [44], MN15 [39], BMK [45], and PW6B95 [46]. All calculations have been performed in conjunction with the def2-QZVPP basis set [47]. With the exception of the Minnesota functionals, which account for dispersion in the functional form, the empirical D3 dispersion correction has been used in conjunction with the Becke–Johnson damping potential (denoted by D3BJ) [48–50].

3. Results and Discussion

[5.5.5.5]hexaene (**1**, Scheme 1) has the molecular formula of $C_{13}H_8$, Scheme 2 depicts key structural $C_{13}H_8$ isomers **2**–**14** that have been identified using the ChemSpider database [51]. [5.5.5.5]hexaene and the $C_{13}H_8$ isomers in Scheme 2 are, by definition, highly unsaturated. As such, most of the $C_{13}H_8$ isomers are polyynes (isomers **2**–**12**, Scheme 2), and many isomers include a phenyl ring (isomers **2**–**10** and **13**, Scheme 2). Isomer **1** does

not contain a phenyl ring; however, it contains a nonplanar conjugated π-system. Therefore, [5.5.5.5]hexaene is expected to be relatively stable compared to the isomers in Scheme 2. Yet, to the best of our knowledge, [5.5.5.5]hexaene (**1**) has not been synthesized; however, several of the $C_{13}H_8$ isomers are synthetically accessible, for example, isomers **2** and **3** [52–54]. In the present work, we examine the relative stability of the $C_{13}H_8$ isomers and show that [5.5.5.5]hexaene (**1**) is the energetically most stable isomer within this space of highly unsaturated structures. This stability may be attributed to the conjugated [12]annulene ring. We also show that, with the exception of isomer **13**, which contains a highly strained cyclobutene ring, all of the isomers that contain a phenyl ring are relatively stable with isomerization energies of ΔH_{298} = 17.5–52.8 kJ mol^{-1} relative to isomer **1**. For example, isomers **2** and **3** are associated with isomerization energies of 17.5 and 24.3 kJ mol^{-1}, respectively, relative to isomer **1**.

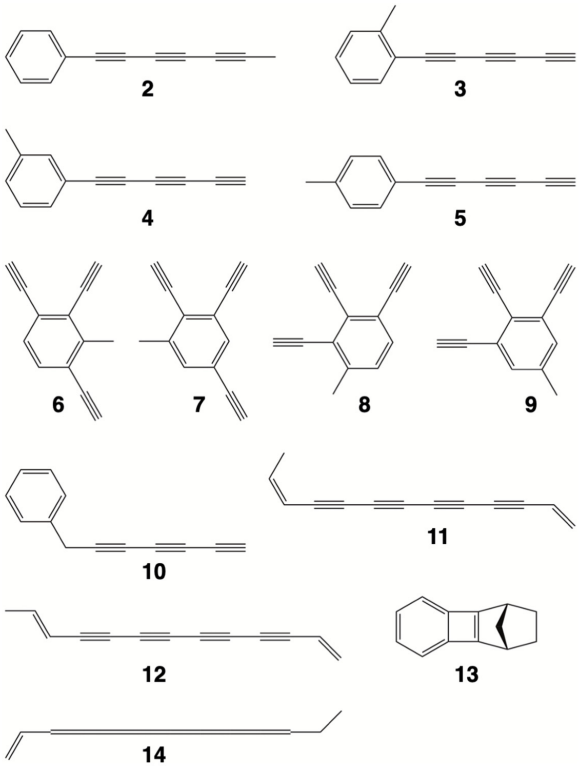

Scheme 2. Illustration of key $C_{13}H_8$ isomers taken from the ChemSpider database.

Table 1 gives the G4 isomerization energies on the electronic (ΔE_e), enthalpic at 0 K (ΔH_0), and enthalpic at 298 K (ΔH_{298}) potential energy surfaces (PESs). Remarkably, our G4 calculations show that **1** is the energetically most stable isomer on the ΔE_e, ΔH_0, and ΔH_{298} PESs. From here onwards, we will focus on the ΔH_{298} values; however, we note that the same trends are observed on the ΔE_e and ΔH_0 PESs. We also note that there is a reasonably good agreement between the G4 and G4(MP2) values. For example, the largest deviation of 12.7 kJ mol^{-1} between the two theories is obtained for isomer **14**. All the G4(MP2) isomerization energies are given in Table S1 of the Supporting Information. All the isomers **2**–**10** contain an aromatic phenyl ring with one (or more) linear acetylenic carbon chain. Isomer **2**, which contains a single $(-C{\equiv}C-)_3$ chain terminated with a methyl group, is less stable than [5.5.5.5]hexaene (**1**) by 17.5 kJ mol^{-1}. Moving the methyl group to the Ph ring in the ortho, meta, and para positions relative to the acetylenic chain (isomers **3**–**5**) destabilizes the isomers. In particular, we obtain isomerization energies of 24.3 (**3**), 28.0 (**5**), and 28.3 (**4**) kJ mol^{-1} relative to isomer **1**. Isomers **6**–**9** all involve three acetylene substituents and one methyl substituent. These isomers, along with isomer **10**, are energetically less stable than isomer **1** by 46.8–52.8 kJ mol^{-1}. All the other isomers

(**11**–**14**) involve long acetylenic or cumulenic chains or a highly strained cyclobutene ring. These isomers are highly energetic and lie as much as 277.3–488.2 kJ mol^{-1} above isomer **1**.

Table 1. CCSD(T) energies relative to isomer **1** (in kJ mol^{-1}) obtained from G4 theory for the fourteen $C_{13}H_8$ isomers shown in Schemes 1 and 2 and transition structures in Figure 1.

Struct.	ΔE_e	ΔH_0	ΔH_{298}	Struct.	ΔE_e	ΔH_0	ΔH_{298}
1	0.0	0.0	0.0	**10**	52.3	43.1	51.4
2	15.3	8.1	17.5	**9**	61.2	42.0	52.8
3	25.8	15.2	24.3	**11**	281.8	263.2	277.3
5	29.5	18.3	28.0	**12**	283.6	264.3	278.7
4	29.8	18.7	28.3	**13**	363.6	359.9	361.4
6	54.9	36.3	46.8	**14**	498.7	472.8	488.2
7	54.8	36.7	46.9	**1-TS$_{inv}$** [a]	262.7	247.5	249.2
8	57.4	38.5	48.9	**1-TS$_{shift}$** [b]	74.6	68.4	67.6

[a] transition structure of 1 for skeletal inversion (see Figure 1b and Scheme 3a). [b] transition structure of 1 for π-bond shift (see Figure 1c and Scheme 3b).

Having established that [5.5.5.5]hexaene (**1**) is a relatively stable $C_{13}H_8$ isomer, it is of interest to examine its structure in more detail. This is a symmetric molecule of D_2 symmetry. The bond lengths and angles are shown in Figure 1a. We begin by noting that even though [5.5.5.5]hexaene is highly nonplanar, the double and single bonds of the outer [12]annulene ring exhibit bond length alternation, indicating a partly delocalized π-system. The double C=C bonds are of similar lengths to those of typical C=C bonds, namely, 1.360 and 1.343 Å, and the single C–C bonds are shorter than typical single C–C bonds, namely, 1.441 and 1.468 Å (Figure 1). For comparison, the length of the conjugated double bonds in cyclopentadiene is 1.346 Å, i.e., in between the lengths of the double bonds in **1**, and the length of the single bond sandwiched between the two double bonds in cyclopentadiene is 1.468 Å.

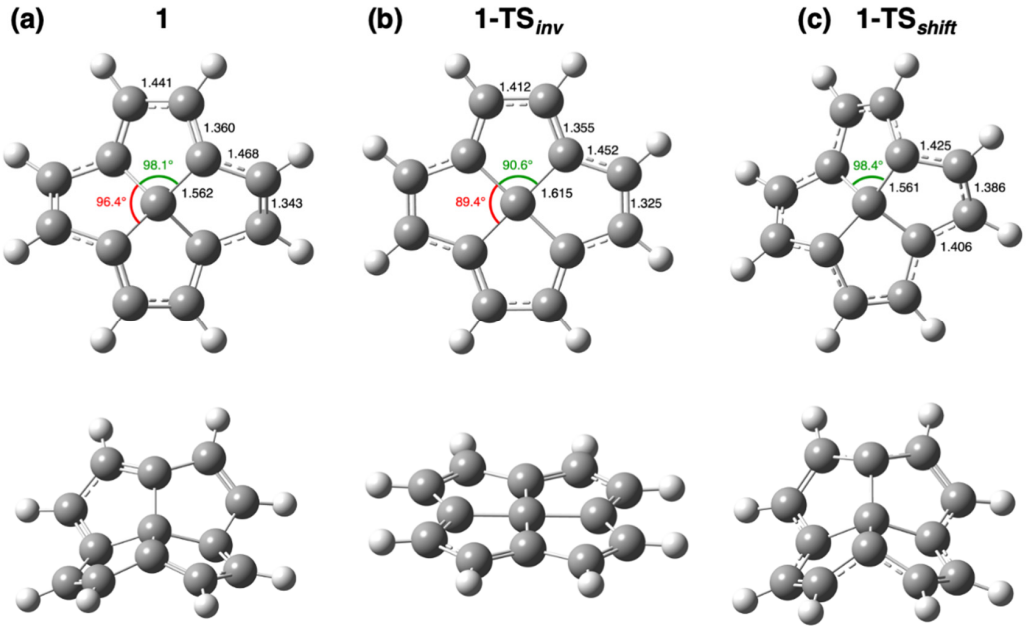

Figure 1. Top and side views of the optimized B3LYP/6-31G(2df,p) structures of (**a**) 1 ([5.5.5.5]hexaene, D_2 symmetry), (**b**) planar transition structure for structural inversion of **1-TS$_{inv}$** (D_{2h} symmetry), and (**c**) transition structure for the double-bond shift in **1-TS$_{shift}$** (C_{2v} symmetry); bond lengths are given in Å (black font), and angles are given in degrees (green and red font). See Table 1 for the relative G4 enthalpies at 298 K.

[5.5.5.5]hexaene and related systems have been initially proposed in the quest to form a tetracoordinate carbon with a planar configuration [1–4,55–57]. Indeed, the outer conjugated annulene imposes, to some extent, a planar configuration around the central sp^3 carbon. This is demonstrated by bond angles around this carbon being smaller than the ideal tetrahedral angle. The two bond angles around the central carbon are 96.4° and 98.1°. The planarity of the central carbon can be assessed by examining the angle between the planes of the two opposite cyclopentadiene rings, which is 56.0° (cfr. to an angle of 90° in a perfect tetrahedral configuration). We note that the angle between the planes of the two opposite cyclopentene rings is very similar and amounts to 56.9°.

The above geometrical parameters show that the central carbon in [5.5.5.5]hexaene is closer to planarity than a tetrahedral carbon; it is therefore of interest to examine the reaction barrier height for the skeletal inversion in this structure. The inversion transition structure is completely planar and has a D_{2h} symmetry (see Figure 1b and Scheme 3a). The four bonds between the central carbon and the carbons of the [12]annulene ring are significantly elongated relative to the equilibrium structure (**1**, Figure 1a). All of the bonds of the [12]annulene ring are slightly shortened relative to the equilibrium structure; therefore, the bond length alternation in the [12]annulene ring is maintained. As expected, the skeletal inversion has a high barrier height of $\Delta H^{\ddagger}_{298}$ = 249.2 kJ mol^{-1} at the G4 level, demonstrating the high configurational stability of [5.5.5.5]hexaene towards skeletal inversion. The high energy of the planar TS for the skeletal inversion may be attributed to two factors: (i) the strain energy associated with a planar structure of four fused five-membered rings sharing a central carbon atom, and (ii) the antiaromaticity of this planar TS, which involves 12 (*4n*) π-electrons [5,58].

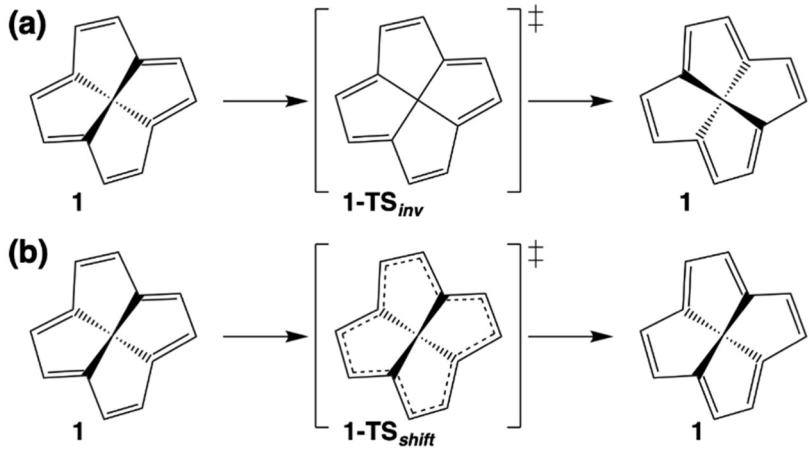

Scheme 3. Schematic illustration of the (**a**) skeletal inversion (**1-TS**$_{inv}$) and (**b**) π-bond shift (**1-TS**$_{shift}$) reactions in [5.5.5.5]hexaene.

It is of interest to examine whether the conjugated [12]annulene ring can undergo a π-bond shift reaction (illustrated schematically in Scheme 3). Figure 1c shows the optimized transition structure for this reaction. The geometric configuration of the central carbon atom in this transition structure is very similar to that in the equilibrium structure. The bond length alternation in this TS is significantly reduced, with the difference in length between the two types of bonds being merely 0.039 Å. The activation energy for the π-bond shift reaction is $\Delta H^{\ddagger}_{298}$ = 67.6 kJ mol^{-1} at the G4 level. Therefore, this process is expected to proceed rapidly at room temperature.

Finally, it is useful to examine the performance of a representative selection of DFT methods across the rungs of Jacob's Ladder in order to accommodate future computational investigations of larger fragments of penta-graphene and related structures. Table 2 gives the root mean square deviations (RMSDs), mean absolute deviations (MADs), mean signed deviations (MSDs), and largest deviations (LDs) for the considered DFT methods. We begin by noting that highly unsaturated hydrocarbons have been shown to be an extremely

challenging target for most DFT functionals [20,59]. Let us begin with examining the performance of the pure GGA methods. BLYP-D3BJ results in an unacceptably large RMSD of 87.7 kJ mol^{-1}, which is mostly attributed to the poor performance of the LYP correlation functional. Replacing the LYP functional with either the P86 or PBE correlation functionals results in significant improvements in performance. Namely, the BP86-D3BJ and BPBE-D3BJ methods result in RMSDs of 27.8 and 23.6 kJ mol^{-1}, respectively. We note that PBE-D3BJ results in a similar performance to BP86-D3BJ, albeit PBE-D3BJ is associated with a much smaller MSD of merely −2.2 kJ mol^{-1} (Table 2). The considered meta-GGA methods (TPSS-D3BJ and MN15-L) do not offer an improvement over the best-performing GGA methods. Moving on to the hybrid-GGA methods, B3LYP-D3BJ shows poor performance, which is considerably improved by the range-separated CAM-B3LYP method. PBE0-D3BJ results in an RMSD of 23.1 kJ mol^{-1}, which is a noticeable improvement over the pure PBE-D3BJ method. Overall, the hybrid-GGA B3PW91-D3BJ provides the best performance of all the considered DFT methods with an RMSD of 14.9 kJ mol^{-1}. Moving on to the hybrid meta-GGA methods, M06-2X provides poor performance with an RMSD of 47.9 kJ mol^{-1}. Interestingly, its predecessor M05-2X results in an RMSD of just 22.0 kJ mol^{-1}. We note that both M05-2X and M06-2X include similar amounts of exact Hartree–Fock exchange, namely, 56% and 54%, respectively. However, M06-2X is more heavily parametrized than M05-2X, which seems to work less well for the highly challenging isomerization energies at hand. Both MN15 and PW6B95-D3BJ do not offer an improvement over the performance of M05-2X. However, BMK-D3BJ results in a significantly lower RMSD of 16.2 kJ mol^{-1} (which is similar to that of B3PW91-D3BJ for which we obtain an RMSD of 14.9 kJ mol^{-1}).

Table 2. Statistical analysis for the performance of selected DFT procedures for calculating the relative energies of the isomers in Scheme 2 relative to the electronic ΔE_e reference values from G4 theory (in kJ mol^{-1}) [a,b].

	RMSD	MAD	MSD	LD
BLYP-D3BJ	87.7	79.8	−76.2	−143.4
BP86-D3BJ	27.8	24.3	−11.0	−52.2
PBE-D3BJ	27.4	24.1	−2.2	−42.5
BPBE-D3BJ	23.6	19.9	1.8	−34.2
TPSS-D3BJ	38.4	32.8	−26.3	−69.6
MN15-L	30.6	27.9	−16.9	−58.7
B3LYP-D3BJ	62.0	57.9	−54.1	−91.8
CAM-B3LYP-D3BJ	38.5	37.0	−35.1	−50.2
PBE0-D3BJ	23.1	17.8	17.4	38.8
B3PW91-D3BJ	14.9	13.3	2.7	22.0
M06-2X	47.9	45.7	−45.7	−61.3
MN15	24.7	22.6	−22.6	−36.5
PW6B95-D3BJ	28.8	22.8	−22.8	−46.8
M05-2X	22.0	20.7	−19.8	−34.0
BMK-D3BJ	16.2	15.2	11.5	−22.2

[a] RMSD = root mean square deviation, MAD = mean absolute deviation, MSD = mean signed deviation, and LD = largest deviation. [b] the cumulenic isomer **14** is highly challenging for DFT methods and is excluded from the evaluation dataset.

4. Conclusions

In this work, we use the high-level G4 composite ab initio method to investigate the thermodynamic and kinetic properties of the smallest prototypical hyperbolic paraboloidal hydrocarbon—[5.5.5.5]hexaene (**1**). We find that this system is energetically stable relative to its isomeric forms. For example, isomers containing a phenyl ring with one or more acetylenic side chains are higher in energy on the enthalpic potential energy surface at 298 K by ΔH_{298} = 17.5–51.4 kJ mol^{-1}, whereas long acetylenic carbon chains are higher in energy by as much as ΔH_{298} = 277.3–488.2 kJ mol^{-1}. [5.5.5.5]hexaene can undergo skeletal inversion via a completely planar transition structure; however, the activation energy for this process is relatively high, being $\Delta H^{\ddagger}_{298}$ = 249.2 kJ mol^{-1} at the G4 level.

This demonstrates the high structural stability of [5.5.5.5]hexaene. Finally, we find that the transition structure for the π-bond shift reaction of the conjugated [12]annulene ring is relatively low-lying with an activation energy of $\Delta H^{\ddagger}_{298}$ = 67.6 kJ mol^{-1}. Therefore, this process is expected to proceed rapidly at room temperature. We hope that these accurate theoretical results will inspire further experimental explorations of [5.5.5.5]hexaene.

Supplementary Materials: The following supporting information can be downloaded at https://www.mdpi.com/article/10.3390/c9020041/s1: G4(MP2) reaction energies and barrier heights for all the reactions considered in the present work (Table S1); optimized geometries for all the species considered in this work (Table S2).

Funding: This research received no external funding.

Data Availability Statement: The data that support the findings of this study are available in the supplementary material of this article and from the corresponding author upon reasonable request.

Acknowledgments: We gratefully acknowledge the generous allocation of computing time from the National Computational Infrastructure (NCI) National Facility, and system administration support provided by the Faculty of Science Agriculture Business and Law to the Linux cluster of the Karton group.

Conflicts of Interest: The author declares no conflict of interest.

References

1. Hoffmann, R.; Alder, R.W.; Wilcox, C.F. Planar tetracoordinate carbon. *J. Am. Chem. Soc.* **1970**, *92*, 4992. [CrossRef]
2. Chandrasekhar, J.; Wurthwein, E.-U.; Schleyer, P.V.R. On the planarity of tetracoordinate carbon enclosed by annulene perimeters. *Tetrahedron* **1981**, *37*, 921. [CrossRef]
3. Minkin, V.I.; Minyaev, R.M.; Hoffmann, R. Non-classical structures of organic compounds: Unusual stereochemistry and hypercoordination. *Russ. Chem. Rev.* **2002**, *71*, 869. [CrossRef]
4. Keese, R. Carbon Flatland: Planar Tetracoordinate Carbon and Fenestranes. *Chem. Rev.* **2006**, *106*, 4787. [CrossRef] [PubMed]
5. Spitler, E.L.; Johnson, C.A.; Haley, M.M. Renaissance of Annulene Chemistry. *Chem. Rev.* **2006**, *106*, 5344. [CrossRef] [PubMed]
6. Pellegrino, S. On the Rigidity of Triangulated Hyperbolic Paraboloids. *Proc. R. Soc. Land. A* **1988**, *418*, 425.
7. Ten, L.V. Rigidity of complete surfaces of negative curvature that coincide with a hyperbolic paraboloid outside a compact region. *Russ. Math. Surv.* **1980**, *35*, 111. [CrossRef]
8. Nazir, M.A.; Hassan, A.; Shen, Y.; Wang, Q. Research progress on penta-graphene and its related materials: Properties and applications. *Nano Today* **2022**, *44*, 101501. [CrossRef]
9. Zhang, S.; Zhou, J.; Wang, Q.; Chen, X.; Kawazoe, Y.; Jena, P. Penta-graphene: A new carbon allotrope. *Proc. Natl. Acad. Sci. USA* **2015**, *112*, 2372. [CrossRef]
10. Cramer, C.J. *Essentials of Computational Chemistry: Theories and Models*, 2nd ed.; Wiley: Hoboken, NJ, USA, 2004.
11. Levine, I.N. *Quantum Chemistry*, 7th ed.; Prentice Hall: New York, NY, USA, 2013.
12. Karton, A. Quantum mechanical thermochemical predictions 100 years after the Schrödinger equation. *Annu. Rep. Comput. Chem.* **2022**, *18*, 123.
13. Karton, A. A computational chemist's guide to accurate thermochemistry for organic molecules. *WIREs Comput. Mol. Sci.* **2016**, *6*, 292. [CrossRef]
14. Curtiss, L.A.; Redfern, P.C.; Raghavachari, K. Gaussian-4 theory. *J. Chem. Phys.* **2007**, *126*, 084108. [CrossRef] [PubMed]
15. Curtiss, L.A.; Redfern, P.C.; Raghavachari, K. Gaussian-4 theory using reduced order perturbation theory. *J. Chem. Phys.* **2007**, *127*, 124105. [CrossRef] [PubMed]
16. Curtiss, L.A.; Redfern, P.C.; Raghavachari, K. Gn Theory. *WIREs Comput. Mol. Sci.* **2011**, *1*, 810. [CrossRef]
17. Zheng, J.; Zhao, Y.; Truhlar, D.G. The DBH24/08 Database and Its Use to Assess Electronic Structure Model Chemistries for Chemical Reaction Barrier Heights. *J. Chem. Theory Comput.* **2009**, *5*, 808. [CrossRef] [PubMed]
18. Curtiss, L.A.; Redfern, P.C.; Raghavachari, K. Assessment of Gaussian-4 theory for energy barriers. *Chem. Phys. Lett.* **2010**, *499*, 168. [CrossRef]
19. Karton, A.; O'Reilly, R.J.; Radom, L. Assessment of theoretical procedures for calculating barrier heights for a diverse set of water-catalyzed proton-transfer reactions. *J. Phys. Chem. A* **2012**, *116*, 4211. [CrossRef]
20. Karton, A.; Martin, J.M.L. Explicitly correlated benchmark calculations on C_8H_8 isomer energy separations: How accurate are DFT, double-hybrid and composite ab initio procedures? *Mol. Phys.* **2012**, *110*, 2477. [CrossRef]
21. Yu, L.-J.; Karton, A. Assessment of theoretical procedures for a diverse set of isomerization reactions involving double-bond migration in conjugated dienes. *Chem. Phys.* **2014**, *441*, 166. [CrossRef]
22. Karton, A.; Goerigk, L. Accurate reaction barrier heights of pericyclic reactions: Surprisingly large deviations for the CBS-QB3 composite method and their consequences in DFT benchmark studies. *J. Comput. Chem.* **2015**, *36*, 622. [CrossRef]

23. Yu, L.J.; Sarrami, F.; O'Reilly, R.J.; Karton, A. Reaction barrier heights for cycloreversion of heterocyclic rings: An Achilles' heel for DFT and standard ab initio procedures. *Chem. Phys.* **2015**, *458*, 1–8. [CrossRef]
24. Karton, A.; Schreiner, P.R.; Martin, J.M.L. Heats of formation of platonic hydrocarbon cages by means of high-level thermochemical procedures. *J. Comput. Chem.* **2016**, *37*, 49. [CrossRef] [PubMed]
25. Karton, A. How reliable is DFT in predicting the relative energies of polycyclic aromatic hydrocarbon isomers? Comparison of functionals from different rungs of Jacob's Ladder. *J. Comput. Chem.* **2017**, *38*, 370. [CrossRef]
26. Karton, A.; Sylvetsky, N.; Martin, J.M.L. W4-17: A diverse and high-confidence dataset of atomization energies for benchmarking high-level electronic structure methods. *J. Comput. Chem.* **2017**, *38*, 2063. [CrossRef]
27. Karton, A. Fullerenes Pose a Strain on Hybrid Density Functional Theory. *J. Phys. Chem. A* **2022**, *126*, 4709. [CrossRef]
28. Lee, C.; Yang, W.; Parr, R.G. Development of the Colle-Salvetti correlation-energy formula into a functional of the electron density. *Phys. Rev. B* **1988**, *37*, 785. [CrossRef] [PubMed]
29. Becke, A.D. Density-functional thermochemistry. III. The role of exact exchange. *J. Chem. Phys.* **1993**, *98*, 5648. [CrossRef]
30. Stephens, P.J.; Devlin, F.J.; Chabalowski, C.F.; Frisch, M.J. Ab Initio Calculation of Vibrational Absorption and Circular Dichroism Spectra Using Density Functional Force Fields. *J. Phys. Chem.* **1994**, *98*, 11623. [CrossRef]
31. Gonzalez, C.; Schlegel, H.B. An improved algorithm for reaction path following. *J. Chem. Phys.* **1989**, *90*, 2154. [CrossRef]
32. Gonzalez, C.; Schlegel, H.B. Reaction path following in mass-weighted internal coordinates. *J. Chem. Phys.* **1990**, *94*, 5523. [CrossRef]
33. Frisch, M.J.; Trucks, G.W.; Schlegel, H.B.; Scuseria, G.E.; Robb, M.A.; Cheeseman, J.R.; Scalmani, G.; Barone, V.; Mennucci, B.; Petersson, G.A.; et al. *Gaussian 16, Revision E.01*; Gaussian, Inc.: Wallingford, CT, USA, 2016.
34. Perdew, J.P.; Schmidt, K. Jacob's ladder of density functional approximations for the exchange-correlation energy. *AIP Conf. Proc.* **2000**, *577*, 1–20.
35. Becke, A.D. Density-functional exchange-energy approximation with correct asymptotic behavior. *Phys. Rev. A* **1988**, *38*, 3098. [CrossRef] [PubMed]
36. Perdew, J.P.; Burke, K.; Ernzerhof, M. Generalized Gradient Approximation Made Simple. *Phys. Rev. Lett.* **1996**, *77*, 3865. [CrossRef]
37. Perdew, J.P. Density-functional approximation for the correlation energy of the inhomogeneous electron gas. *Phys. Rev. B* **1986**, *33*, 8822. [CrossRef] [PubMed]
38. Tao, J.M.; Perdew, J.P.; Staroverov, V.N.; Scuseria, G.E. Climbing the Density Functional Ladder: Nonempirical Meta–Generalized Gradient Approximation Designed for Molecules and Solids. *Phys. Rev. Lett.* **2003**, *91*, 146401. [CrossRef]
39. Yu, H.S.; He, X.; Li, S.L.; Truhlar, D.G. MN15: A Kohn–Sham global-hybrid exchange–correlation density functional with broad accuracy for multi-reference and single-reference systems and noncovalent interactions. *Chem. Sci.* **2016**, *7*, 5032. [CrossRef] [PubMed]
40. Perdew, J.P.; Chevary, J.A.; Vosko, S.H.; Jackson, K.A.; Pederson, M.R.; Singh, D.J.; Fiolhais, C. Atoms, molecules, solids, and surfaces: Applications of the generalized gradient approximation for exchange and correlation. *Phys. Rev. B* **1992**, *46*, 6671. [CrossRef]
41. Adamo, C.; Barone, V. Toward reliable density functional methods without adjustable parameters: The PBE0 model. *J. Chem. Phys.* **1999**, *110*, 6158. [CrossRef]
42. Yanai, T.; Tew, D.; Handy, N.C. A new hybrid exchange–correlation functional using the Coulomb-attenuating method (CAM-B3LYP). *Chem. Phys. Lett.* **2004**, *393*, 51. [CrossRef]
43. Zhao, Y.; Schultz, N.E.; Truhlar, D.G. Design of Density Functionals by Combining the Method of Constraint Satisfaction with Parametrization for Thermochemistry, Thermochemical Kinetics, and Noncovalent Interactions. *J. Chem. Theory Comput.* **2006**, *2*, 364. [CrossRef]
44. Zhao, Y.; Truhlar, D.G. The M06 suite of density functionals for main group thermochemistry, thermochemical kinetics, noncovalent interactions, excited states, and transition elements: Two new functionals and systematic testing of four M06-class functionals and 12 other functionals. *Theor. Chem. Acc.* **2008**, *120*, 215.
45. Boese, A.D.; Martin, J.M.L. Development of density functionals for thermochemical kinetics. *J. Chem. Phys.* **2004**, *121*, 3405. [CrossRef] [PubMed]
46. Zhao, Y.; Truhlar, D.G. Design of Density Functionals That Are Broadly Accurate for Thermochemistry, Thermochemical Kinetics, and Nonbonded Interactions. *J. Phys. Chem. A* **2005**, *109*, 5656. [CrossRef] [PubMed]
47. Weigend, F.; Ahlrichs, R. Balanced basis sets of split valence, triple zeta valence and quadruple zeta valence quality for H to Rn: Design and assessment of accuracy. *Phys. Chem. Chem. Phys.* **2005**, *7*, 3297. [CrossRef] [PubMed]
48. Grimme, S.; Antony, J.; Ehrlich, S.; Krieg, H. A consistent and accurate ab initio parametrization of density functional dispersion correction (DFT-D) for the 94 elements H-Pu. *J. Chem. Phys.* **2010**, *132*, 154104. [CrossRef] [PubMed]
49. Grimme, S.; Ehrlich, S.; Goerigk, L. Effect of the damping function in dispersion corrected density functional theory. *J. Comput. Chem.* **2011**, *32*, 1456. [CrossRef] [PubMed]
50. Becke, A.D.; Johnson, E.R. A density-functional model of the dispersion interaction. *J. Chem. Phys.* **2005**, *123*, 154101. [CrossRef]
51. The $C_{13}H_8$ Isomers Were Identified Using the ChemSpider Database. ChemSpider Is a Comprehensive Freely Available Database with over 100 Million Chemical Structures. Available online: http://www.chemspider.com (accessed on 1 January 2023).

52. Sorensen, J.S.; Sorensen, N.A. Studies Related to Naturally Occurring Acetylene Compounds. XXII* Correctional Studies on the Constitution of the Polyacetylenes of some Annual Coreopsis Species. *Acta Chem. Scand.* **1958**, *12*, 756. [CrossRef]
53. Akiyama, S.; Misumi, S.; Nakagawa, M. Cyclic Acetylenes. IX. Synthesis of a Cyclic Octaacetylene Containing Anthracene Nuclei. *Bull. Chem. Soc. Jpn.* **1962**, *35*, 1829. [CrossRef]
54. Jones, E.R.H.; Skattebøl, L.; Whiting, M.C. Researches on acetylenic compounds. Part LX. The synthesis of three natural polyacetylenic hydrocarbons. *J. Chem. Soc.* **1958**, 1054. [CrossRef]
55. Keese, R.; Pfenninger, A.; Roesle, A. Planarization of Tetracoordinate Carbon Atom. Synthesis of 13-oxa-14-oxo-pentacyclo [5.5.2.1.04,15010,15]pentadecane, a bridged 'tetraquinacane'. *Helv. Chim. Acta* **1979**, *62*, 326. [CrossRef]
56. Bohm, M.C.; Gleiter, R.; Schang, P. On the planarity of tetracyclo [5.5.1.$0^{4,13}$o^{10,13}] tridecahexaene. *Tetrahedron Lett.* **1979**, *20*, 2575. [CrossRef]
57. Kubiak, G.G.I. Mechanistic and Synthetic Studies on the Scope of the Weiss Reaction. II. Studies Directed toward the Preparation of Staurane-1,3,5,7,9,11-Hexaene on the Route towards Tetracoordinate Planar Carbon. Ph.D. Thesis, The University of Wisconsin, Milwaukee, WI, USA, 1989. Available online: https://www.proquest.com/docview/303806144?pq-origsite=gscholar&fromopenview=true (accessed on 1 January 2023).
58. Klärner, F.-G. About the Antiaromaticity of Planar Cyclooctatetraene. *Angew. Chem. Int. Ed.* **2001**, *40*, 3977. [CrossRef]
59. Karton, A.; Tarnopolsky, A.; Martin, J.M.L. Atomization energies of the carbon clusters C_n (n = 2–10) revisited by means of W4 theory as well as density functional, G*n*, and CBS methods. *Mol. Phys.* **2009**, *107*, 977. [CrossRef]

Disclaimer/Publisher's Note: The statements, opinions and data contained in all publications are solely those of the individual author(s) and contributor(s) and not of MDPI and/or the editor(s). MDPI and/or the editor(s) disclaim responsibility for any injury to people or property resulting from any ideas, methods, instructions or products referred to in the content.